atmosphere

MDPI

Article

Causes Investigation of $PM_{2.5}$ and O_3 Complex Pollution in a Typical Coastal City in the Bohai Bay Region of China in Autumn: Based on One-Month Continuous Intensive Observation and Model Simulation

Yuanyuan Ji [1], Cong An [1], Jinghao Tang [2], Jialin Li [3], Xiaoyu Yan [1], Xiaoshuai Gao [1], Wanghui Chu [1], Xuelian Zhong [2], Fanyi Shang [4], Jidong Li [4], Luyao Tan [5], Rui Gao [1], Fang Bi [1] and Hong Li [1,*]

[1] State Key Laboratory of Environmental Criteria and Risk Assessment, Chinese Research Academy of Environmental Sciences, Beijing 100012, China; ji.yuanyuan@craes.org.cn (Y.J.)
[2] Environment Research Institute, Shandong University, Qingdao 266000, China
[3] State Key Laboratory of Atmospheric Boundary Layer Physics and Atmospheric Chemistry, Institute of Atmospheric Physics, Chinese Academy of Sciences, Beijing 100029, China
[4] Dongying Municipal Ecology and Environment Bureau, Dongying 257000, China
[5] Ltd. of Shandong Environmental Protection Industry Corp., Jinan 250000, China
* Correspondence: lihong@craes.org.cn

Abstract: In order to investigate the causes of complex air pollution in coastal cities in the Bohai Rim of China, a one-month intensive field observation combined with model simulation was carried out in a typical city named Dongying in September 2022. The results showed that two $PM_{2.5}$ and O_3 complex pollution episodes occurred in Dongying in the observation period, with the primary pollutant being O_3. Atmospheric photochemical reactions occurring under unfavorable meteorological conditions led to the production of O_3 while at the same time facilitating the generation of nitrate, sulfate, and other secondary components of $PM_{2.5}$ by enhancing the atmospheric oxidizing capacity, which promoted the formation of complex air pollution. It was worth noting that in the context of high pollutants emission, the occurrence of complex air pollution was more sensitive to the variation in meteorological conditions than to the change in pollutants emission. To continuously improve air quality and protect human health in Dongying, it is recommended that an effective regional joint air pollution prevention and control mechanism with neighboring cities should be established in the premise of effective local pollutants reduction, and special attention should be paid to the adverse effect of the air mass transportation from Bohai Bay.

Keywords: $PM_{2.5}$ and O_3; complex air pollution; Bohai Bay region; model simulation

check for updates

Citation: Ji, Y.; An, C.; Tang, J.; Li, J.; Yan, X.; Gao, X.; Chu, W.; Zhong, X.; Shang, F.; Li, J.; et al. Causes Investigation of $PM_{2.5}$ and O_3 Complex Pollution in a Typical Coastal City in the Bohai Bay Region of China in Autumn: Based on One-Month Continuous Intensive Observation and Model Simulation. *Atmosphere* **2024**, *15*, 73. https://doi.org/10.3390/atmos15010073

Academic Editors: Giacomo Alessandro Gerosa and Kumar Vikrant

Received: 30 November 2023
Revised: 25 December 2023
Accepted: 5 January 2024
Published: 7 January 2024

1. Introduction

With the rapid development of the national economy and the acceleration of urbanization, the air pollution problems experienced by developed countries in the past 100 years have occurred in China in the past two or three decades, and are prominently manifested in the emergence of complex air pollution [1,2]. Complex air pollution is a system composed of multiple pollutants of high concentrations at the same time, which are coupled and added under certain meteorological conditions [3,4]. These pollutants come from gaseous and particulate primary pollutants emitted from a variety of pollution sources, as well as secondary pollutants such as sulfate, nitrate, and O_3 formed through a series of physical and chemical processes [5,6]. Under the influence of weather and climate systems, these pollutants form high concentrations of pollutants, which transport and react with each other over a wide range of regions. Complex air pollution is characterized by additive effects of multiple pollution types, coupling of multiple processes, and multi-scale pollution interactions, with a core driving force of atmospheric oxidation, and a representative pollutant of

O_3 [7,8]. $PM_{2.5}$ and O_3 not only harm the ecological environment, but also harm human health. High concentrations of $PM_{2.5}$ can cause cardiovascular diseases and respiratory diseases, and high concentrations of O_3 can irritate the human eyes and cause adverse reactions such as sore throat, chest tightness, shortness of breath, and headache [9–12]. Their interaction can lead to a significant increase in the risk of human death [13].

Since 2013, China has issued air pollution prevention and control measures such as the Action Plan of Air Pollution Prevention and Control (2013–2017) and the Three-Year Action Plan for Winning the Blue-Sky Defense War (2018–2020), which have achieved remarkable results: $PM_{2.5}$ concentrations have dropped significantly, and the number of heavy pollution days has decreased significantly. However, the annual average values of $PM_{2.5}$ in many cities have not yet reached the limit of the secondary standard set out in the National Ambient Air Quality Standard of China (GB 3095-2012), which is 35 $\mu g/m^3$ [14]. Meanwhile, O_3 has become a major pollutant after $PM_{2.5}$, so that although $PM_{2.5}$ concentrations have decreased in many regions of China, the proportion of days with good air quality has not increased, or has even decreased [7]. On the regional scale, the level and scope of O_3 pollution are expanding; on the temporal scale, O_3 pollution is evident in spring, and the polluted months tend to appear earlier [15]. The results show that from 2015 to the second half of 2020, under the background that the number of days with $PM_{2.5}$ exceeding the standard limit decreased year by year, there were still 611 complex pollution station-days with $PM_{2.5}$ and O_3 exceeding the standard limits at the same time, and O_3 was the primary pollutant [16]. In conclusion, $PM_{2.5}$ and O_3 are the main factors affecting air quality in cities and regions of China, and their coordinated control is the focus of continuous improvement of air quality in China. The formation mechanism of $PM_{2.5}$ and O_3 is an important anchor for further control of $PM_{2.5}$ and O_3.

At present, many studies have been carried out on the formation mechanism of $PM_{2.5}$ and O_3. It is believed that there is homology between $PM_{2.5}$ and O_3 pollution and their physical and chemical processes are closely related. Firstly, $PM_{2.5}$ and O_3 have common precursors (NO_x and volatile organic compound (VOCs)) and are both affected by meteorological factors; therefore, they are closely related in terms of pollution causes [17–19]. Secondly, there is also a notable combined interaction between $PM_{2.5}$ and O_3. O_3 has strong oxidation, which has an important effect on the change of atmospheric oxidation, which then significantly affects the formation of secondary components of $PM_{2.5}$. And $PM_{2.5}$ affects O_3 formation by regulating temperature, extinction, and heterogeneous reactions of HO_2 radicals on its surface [20–23]. However, the causes of pollution vary, depending on the geographical locations and industrial structures of different cities. Relevant studies in different regions and cities are helpful to scientifically formulate response measures.

Dongying, Shandong Province, located in the southwest of the Bohai Bay, east of the Bohai Sea, is one of the typical coastal cities around the Bohai Sea. It has a large amount of oil and gas resources, and the petrochemical industry is developed, but it does not have good conditions for port construction, so the transportation of bulk goods mainly depends on road traffic. In terms of urban traffic, the motor vehicle use is high, and there are many transit trucks in the urban area. The typical industrial structure and transportation mode of Dongying City lead to a large emission of NO_x and VOCs [24,25]. Statistically, complex pollution of $PM_{2.5}$ and O_3 often occurred in March, June, September, and October (Figure S1), affecting the improvement of the city's ambient air quality. Therefore, it is necessary to analyze the causes and sources of the complex pollution of $PM_{2.5}$ and O_3 in Dongying City. In September 2022, a comprehensive observation was carried out in Dongying City. This study analyzed the concentrations and variations of pollutants in the process of the complex pollution of $PM_{2.5}$ and O_3, and provided the first comprehensive analysis of the effects of meteorological conditions, pollutant emissions, local chemical transformations, regional contributions, and industry contributions on the $PM_{2.5}$ and O_3 complex pollution based on observations and simulations in Dongying. The results of the study could provide scientific support for the preparation of coordinated prevention and control measures for $PM_{2.5}$ and O_3 pollution and the continuous improvement of ambient air quality in Dongying.

2. Materials and Methods

2.1. Observation Period and Location

Dongying City is located in the southwest of the Bohai Sea and the northwest of Shandong Province, adjacent to the Bohai Sea in the east and north, to Binzhou city in the west, and to Zibo city and Weifang city in the south. Its air quality is often affected by air mass transport over the Bohai Sea, and it can be used as a representative coastal city in the around Bohai Sea region. The routine pollutant monitoring stations in this study are the state-controlled stations (6) and the provincial-controlled stations (8) in Dongying. The enhanced observation station in this study is the Dongying Atmospheric Observatory, which is located at the Dongying District Branch of the Dongying Ecological Environment Bureau (118.59° E, 37.45° N) (Figure 1). The station is mainly surrounded by residential areas and commercial office areas, with convenient transportation and no obvious industrial pollution sources. It is a typical urban station which can accurately reflect the air pollution of Dongying city. The observation period is from 1 September to 30 September 2022.

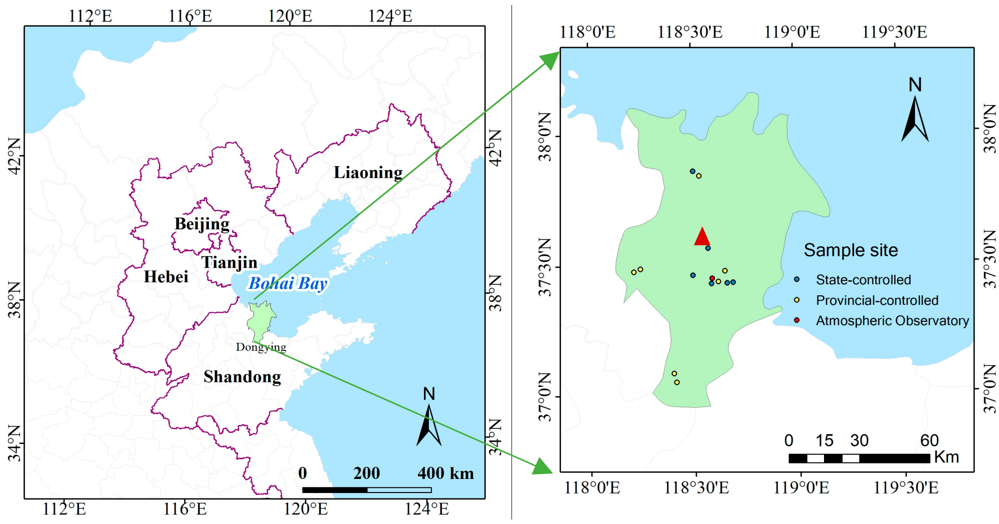

Figure 1. Geographic location of Dongying and locations of the enhanced observation station.

2.2. Observation Items and Quality Control Quality Assurance

The routine observation items include O_3, CO, SO_2, NO, NO_2, and $PM_{2.5}$. The enhanced observation items include routine monitoring parameters (O_3, CO, SO_2, NO, NO_2, and $PM_{2.5}$), 115 VOCs, OC (organic carbon), EC (elemental carbon), ionic components, elements in $PM_{2.5}$, ultraviolet radiation, and meteorological parameters (temperature, relative humidity, atmospheric pressure, wind direction, and wind speed). All observation items were continuously monitored with automatic monitoring devices. SO_2, CO, NO-NO_2-NO_x, and O_3 were monitored with 43i, 48i, 42i, and 49i (Thermo Fisher Scientific Inc., Waltham, MA, USA), respectively. Particulate matters were monitored online with BAM1020 (Met One Instruments Inc., Washington, DC, USA). VOCs were monitored with XHVOC6000 (Hebei Sailhero Environmental Protection Hi-tech., Ltd., Shijiazhuang, Hebei, China). The OC and EC analyzer model was OCEC-100 (Focused Photonics Inc., Hangzhou, Zhejiang, China). The elemental analyzer model was CES Xcat625 (Sailbri Cooper Inc., Tigard, OR, USA). The ion component analyzer model was S−611EG (Zhang Jia Ltd., Taiwan, China). The ultraviolet radiation observer model was Kipp and Zonen SUV-A, SUV-B (OTT HydroMet B.V., Delft, The Netherlands). Meteorological parameters such as temperature and relative humidity were monitored with MULTI/WS-5P (Shenzhen Flying-wis Instrument Equipment Co., Ltd., Shenzhen, Guangdong, China). Vertical distribution characteristics of O_3 and $PM_{2.5}$ were monitored with LGO-01 (Anhui Landun Photoelectron Co., Ltd., Tongling, Anhui, China) and AGHJ-I-LIDAR (Wuxi Zhongke photoelectric Technology Co., Ltd., Wuxi, Anhui, China), respectively. The emission source data were obtained from Dongying environmental automatic monitoring and control system.

The frequency and duration of data collection, quality assurance, and quality control of all observation items met the requirements of the technical specifications such as Automated Methods for Ambient Air Quality Monitoring (HJ/T193-2005), Specifications and Test Procedures for Ambient Air Quality Continuous Monitoring System with Gas Chromatography for Volatile Organic Compounds (HJ 1010-2018), Technical Specifications for Continuous Automated Monitoring of Organic carbon and Elemental Carbon in Ambient Air Particulate Matter ($PM_{2.5}$) (Draft), Technical Specifications for Continuous Automated Monitoring of Water-Soluble Ions in Ambient Air Particulate Matter ($PM_{2.5}$) (Draft), and Technical Specifications for Continuous Automated Monitoring of Inorganic Elements in Ambient Air Particulate Matter ($PM_{2.5}$) (Draft). The values recorded by the devices could be calculated as hourly arithmetic means. Details of the standard operating procedure are available from the Ministry of Environmental Protection of the People's Republic of China (https://www.mee.gov.cn/, accessed on 6 January 2024).

2.3. Data Processing

2.3.1. Pollution Processes Classification

According to the requirements in the Technical Regulation on Ambient Air Quality Index (on trial) (HJ 633-2012) (details are in the Supplementary Material), pollution days in this paper are defined as days with an AQI (air quality index) > 100, while light pollution days are defined as those with 100 < AQI $\leq$ 150 and moderate pollution days as those with 150 < AQI $\leq$ 200. Clean days are defined as having an AQI less than 100. The air quality level was excellent when 0 < AQI $\leq$ 50, and good when 50 < AQI $\leq$ 100. When the AQI was more than 50, the air pollutant with the highest IAQI (air quality sub-index) was called the primary pollutant.

Based on the above definition, combined with the monitoring data from the state-controlled stations in Dongying, there were 15 polluted days and 15 clean days in Dongying in September 2022. Additionally, it can be seen that there were two long pollution periods. Episode I was from 8 to 12 September, dominated by light pollution. Episode II was from 25 to 30 September, dominated by moderate pollution. During the pollution period, the primary pollutant was O_3 (the value of maximum daily 8 h average ozone (MDA8-O_3) > 160 $\mu g/m^3$), with high concentration of $PM_{2.5}$ (>35 $\mu g/m^3$), and the concentrations of other pollutants were also at high levels. It was obviously characterized by complex air pollution.

2.3.2. Inverse Distance Weighted

In order to analyze the spatial distribution of $PM_{2.5}$ and O_3 during the pollution process in September, the $PM_{2.5}$ and O_3 monitoring data from the state-controlled and provincial-controlled stations in Dongying were analyzed by using Inverse Distance Weighted (IDW) in ArcGIS. The principle of IDW is to use surrounding measurements to predict the value at any unsampled location. The method assumes that the closer the distance, the closer the values.

2.3.3. Ozone Integrated Source Apportionment Method

In this paper, source apportionment for O_3 was conducted using air quality model Regional Atmospheric Modeling System-Community Multiscale Air Quality (RAMS-CMAQ), combined with Integrated Source Apportionment Method (ISAM) based on enhanced observational data.

For ISAM, O_3 was identified using tracer methods to track various processes (including source emission, deposition, transmission, diffusion, and chemical changes) of O_3 and its precursors (NO_x and VOCs) in the atmosphere, and then tracer factors were set for different geographical areas or different types of pollution sources according to the needs of the study [26,27]. For this purpose, four classes of tracers, N_i, V_i, O_3N_i, and O_3V_i, were used in ISAM. N_i and V_i were used to trace the nitrogen-containing species and VOCs components, respectively, emitted from source type i (i.e., a certain type of source in a certain area, which can also denote the initial or boundary conditions of the model). O_3N_i and O_3V_i represented the contribution of source type i emissions to O_3 formation under NO_x control and VOCs control, respectively.

The simulated regions set in this study are shown in Figure S2, where the regions within the black box are the main regions of interest, while the 16 regions filled with colors are the marked regions selected for ISAM source apportionment.

2.3.4. Observation-Based Model

Based on enhanced observational data, Observation-Based Model (OBM) was used to simulate the net O_3 formation rate and its sensitivity mechanism in Dongying City. The model uses the Regional Atmospheric Chemistry Mechanism (RACM) v2.0 mechanism to describe 363 chemical reactions of over 50 species and has been widely used in atmospheric chemistry observation and sensitivity simulation studies [28–31].

Relative incremental reactivity (RIR) is defined as the ratio of the percentage change in the net O_3 formation rate (or amount) to the percentage change in the concentration (emission) of a particular species and is used to assess the impact of reduction of specific precursor on the net O_3 formation rate (concentration). In this study, a sensitivity test was performed based on the assumption that each precursor class, such as NO_x, anthropogenic hydrocarbons (AHCs), and biogenic hydrocarbons (BHCs), would be reduced by 20%. The equation for calculating the RIR is as follows:

$$\mathrm{RIR}(X) = \frac{\frac{P_{\mathrm{net-O_3}}(X) - P_{\mathrm{net-O_3}}[X - \Delta S(X)]}{P_{\mathrm{net-O_3}}(X)}}{\frac{\Delta S(X)}{S(X)}}$$

where $P_{\mathrm{net-O3}}(X)$ and $P_{\mathrm{net-O3}}(X)$ $[X - \Delta S(X)]$ are the net O_3 formation rate before and after target precursor emission reduction, respectively, in 10^{-9} h^{-1}; $S(X)$ is the concentration of target precursor before emission reduction, in μg/m^3; $\Delta S(X)$ is the concentration of target precursor after emission reduction, in μg/m^3. When RIR is positive, it indicates that reducing the target precursor emissions can effectively reduce O_3 generation. The higher RIR value is, the more sensitive O_3 formation is to the target precursor. This is reversed for negative RIRs.

2.3.5. Transformation Rate of Sulfates and Nitrates

To further verify the promoting effect of atmospheric oxidation capacity on the transformation of secondary pollutants in ambient air in Dongying, SOR (transformation rate of sulfates) and NOR (transformation rate of nitrates) were used to determine the transformation status of gaseous precursors such as SO_2 and NO_x to form secondary inorganic aerosols. The higher the values of SOR and NOR, the higher the degree of secondary transformation of SO_2 and NO_2 in the atmosphere. The equation is as follows:

$$\mathrm{NOR} = N_1/(N_1 + N_2)$$

$$\mathrm{SOR} = S_1/(S_1 + S_2)$$

where N_1 and N_2 are the concentrations of NO_3^- and NO_2, respectively, in mol/m^3; S_1 and S_2 are the concentrations of SO_4^{2-} and SO_2, respectively, in mol/m^3.

2.3.6. Calculation of Secondary Organic Carbon

In this study, the OC/EC ratio method was used to estimate the mass concentration of SOC (secondary organic carbon) based on the measured concentrations of OC and EC in $PM_{2.5}$. The calculation formula is as follows:

$$SOC = TOC - OC_{pri}$$

$$OC_{pri} = EC \times (OC/EC)_{min}$$

where TOC, EC, and OC_{pri} are the concentrations of OC, EC, and primary organic carbon in $PM_{2.5}$, respectively, in $\mu g/m^3$; $(OC/EC)_{min}$ is minimal ratio of the measured OC concentration to the EC concentration [32].

2.3.7. Backward Trajectory

Among meteorological trajectory model software, the TrajStat model calculates air flow trajectories from meteorological data. There are various air flow tracks at the observation sites. The cluster analysis method can be used to distinguish the trajectories according to their correlation. The air trajectories with higher similarity can be divided into one group in order to obtain the direction and transmission distance of the dominant air during the pollution of the observation site [33].

In this study, the software MeteoInfo 3.7.6 and the TrajStat 1.5.3 plugin were used to investigate the effect of long-distance air mass transport [34]. The 48 h backward trajectories of the sampling site were calculated and clustered, with a height of 100 m. The meteorological data used in the analysis (GDAS) were from ftp://arlftp.arlhq.noaa.gov/pub/archives/gdas1 (accessed on 6 September 2023), mainly including data like temperatures, atmospheric pressures, and wind speeds. The starting time in each day was 00:00 UTC. The simulation frequency was 1 h, and a total of 24 trajectories were calculated each day to obtain the backward trajectories. After the trajectory calculation was completed, cluster analysis of the airflow trajectories was performed using the clustering method in software TrajStat 1.5.3 and the Euclidean distance algorithm. Then, combined with the corresponding pollutant mass concentration characteristics, the statistical analysis was carried out.

3. Results and Discussion

3.1. Air Quality and Meteorological Conditions

In September 2022, there were 15 days of air pollution in Dongying City, of which 11 days were light pollution (5, 8, 10–12, 17, 21–22, 25, and 30 September) and 5 days were moderate pollution (9, 26–29 September) (Figure S3). O_3 was the primary pollutant on all polluted days.

In September 2022, the hourly concentrations of O_3 and $PM_{2.5}$ in the Dongying varied from 8 to 275 $\mu g/m^3$ and 2 to 86 $\mu g/m^3$, respectively (Figure 2). Continuous high concentrations of $PM_{2.5}$ were observed during the period of O_3 pollution from 8 to 12 September and from 25 to 30 September (Figure 2). NO_2 and SO_2 concentrations were also high, with hourly values ranging from 2 to 95 $\mu g/m^3$ and from 4 to 58 $\mu g/m^3$, respectively (Figure 2). In the early stage of complex pollution, the hourly concentrations of NO_2 and SO_2 increased significantly, and the peak concentrations reached several times of those before complex pollution (Figure 2). During the pollution period, the wind speeds of Dongying City were between 0.1 and 1.9 m/s, which was small, and the dominant wind direction was variable, which was not conducive to the diffusion of pollutants (Figure 3). The temperatures and relative humidities ranged from 14.0 °C to 34.4 °C and from 22.8% to 96.7%, respectively, with typical characteristics of high humidity at night and high temperature in daytime, which was conducive to the complex pollution process of $PM_{2.5}$ and O_3 (Figure 3).

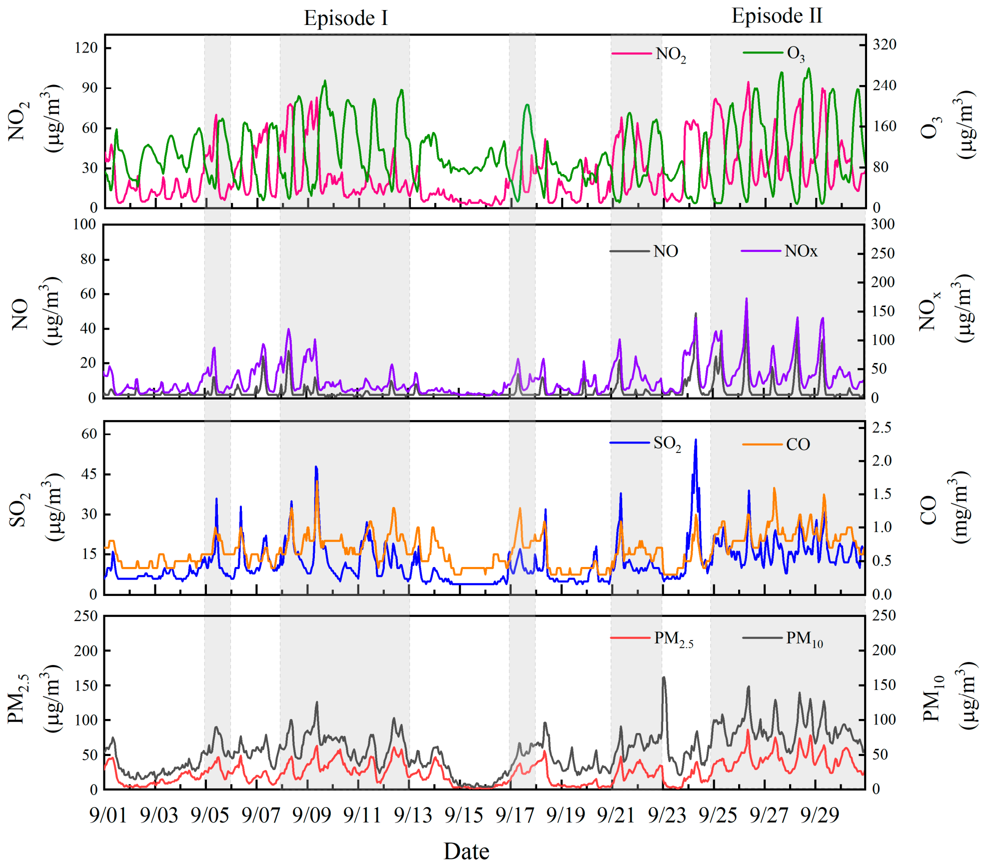

Figure 2. Time series diagram of pollutant concentrations in Dongying in September 2022. The grey part in the figure represents polluted days.

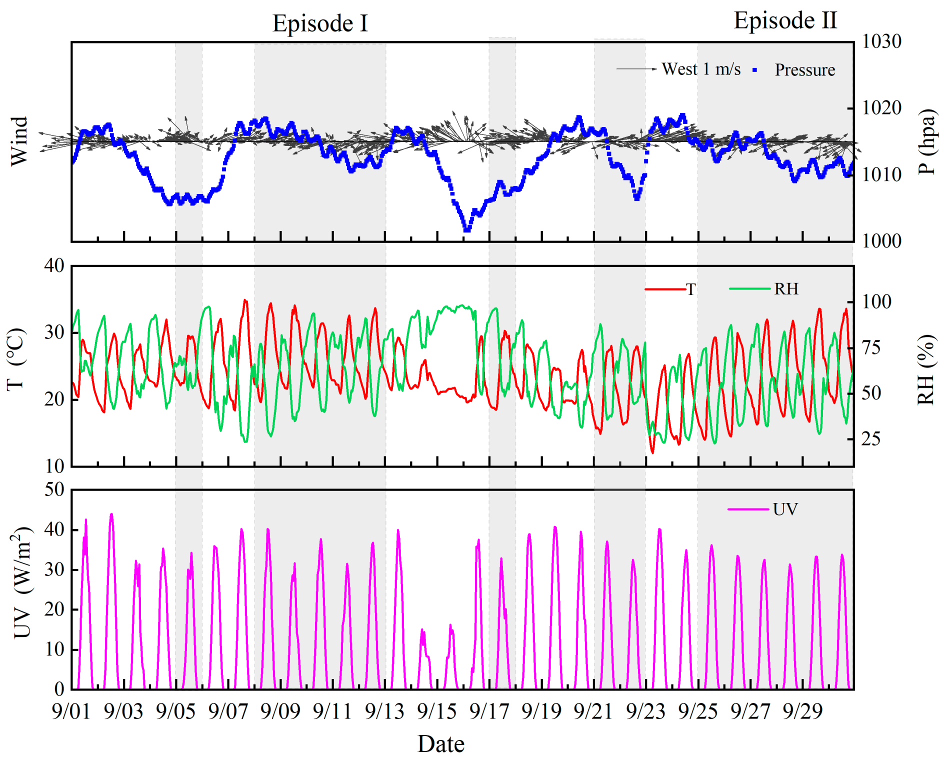

Figure 3. Time series diagram of meteorological factors in Dongying in September 2022. The grey part in the figure represents polluted days.

3.2. Characteristics of Complex Air Pollution

3.2.1. Temporal Variation

In the view of daily variation, the range of $PM_{2.5}$ and MDA8 O_3 were 3–49 μg/m^3 and 82–259 μg/m^3 in Dongying in September 2022, respectively. The maximum values of $PM_{2.5}$ and O_3 appeared on the 28th. During the pollution period from 25th to 30th, the daily values of $PM_{2.5}$ were higher than 35 μg/m^3, and the values of MDA8 O_3 were higher than 160 μg/m^3, showing an obvious complex pollution process (Figure S1).

In the view of hourly concentration (Figure 2), the hourly concentration of O_3 ranged from 8 to 275 μg/m^3 in Dongying in September 2022, which was lower in the beginning and middle of the month and higher at the end of the month. On 1–7, 13–16, 18–20, and 23–24 September, the hourly concentration of O_3 was low, with peaks around and below 150 μg/m^3. On 8–12, 17, 21–22 and 25–30 September, the hourly concentration of O_3 was high, with peaks of approximately 250 μg/m^3 on 9 and 26–28 September. The hourly concentration of $PM_{2.5}$ ranged from 2 to 86 μg/m^3, which was lower at the beginning and the middle of the month, and higher at the end of the month, which was consistent with the hourly concentration of O_3. $PM_{2.5}$ concentrations were low on 2–4, 7, 15–17, 19–20, and 23 September. On 1, 5–6, 8–14, 18 and 21–22, and 24–30 September, hourly $PM_{2.5}$ concentrations were high, with peaks exceeding 40 μg/m^3. The highest hourly concentration of $PM_{2.5}$ was observed from 26 to 28 September, with a peak of 86 μg/m^3. The highest concentrations of O_3 and $PM_{2.5}$ showed a consistent correlation on the polluted days, especially on the moderately polluted days from 26 to 28 September.

In terms of $PM_{2.5}$ components, the concentrations of organic matters, NO_3^-, SO_4^{2-} and NH_4^+ in $PM_{2.5}$ ranged from 0.02 to 29.00 μg/m^3, 0.06 to 34.07 μg/m^3, 0.15 to 19.66 μg/m^3, and 0.29 to 15.97 μg/m^3 in September 2022, respectively (Figure 4). Organic matters accounted for the largest proportion (29.69%), followed by NO_3^- (18.32%), SO_4^{2-} (15.01%), and NH_4^+ (18.32%) (Figure 4).

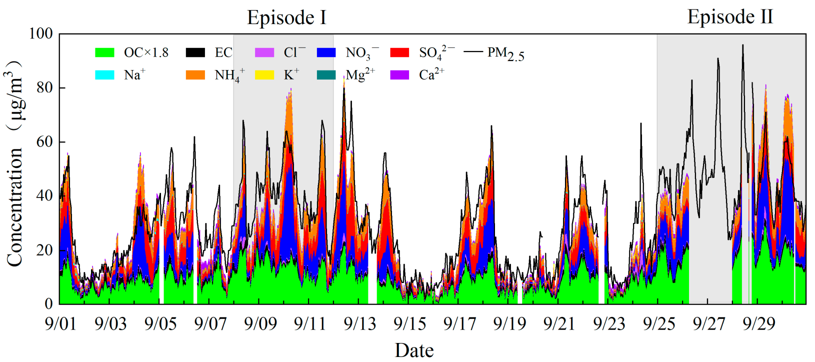

Figure 4. Time series variation of $PM_{2.5}$ components in Dongying in September 2022.

The diurnal variation of O_3 on both polluted and clean days showed a single peak, starting to rise at 07:00 and peaking from 16:00–17:00 before declining (Figure 5a). The solar radiation lasted from 07:00 to 18:00 during the day and decreased to 0 W/m^2 at 19:00. The similarity between the diurnal variation of O_3 concentration and the intensity of solar radiation confirmed that O_3 is strongly influenced by photochemical production (Figure S4). At 9:00, the hourly concentration of O_3 on the polluted and clean days were similar. Before 9:00, the hourly concentration of O_3 on clean days was higher than that on polluted days. After 9:00, the hourly concentration of O_3 was lower on clean days than that on polluted days. In the morning of pollution days, it increased rapidly and reached the peak at 16:00 (over 200 μg/m^3). On the clean days, it increased slowly and peaked at 16:00 and 17:00 (about 100 μg/m^3).

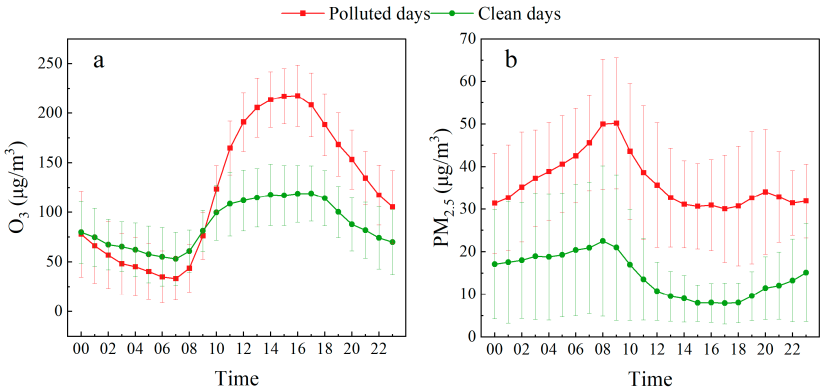

Figure 5. Diurnal variation of the O_3 (**a**) and $PM_{2.5}$ (**b**) concentrations on the polluted and clean days in Dongying in September 2022.

The hourly concentration of $PM_{2.5}$ showed a diurnal variation of first rising and then decreasing (Figure 5b). The hourly concentration of $PM_{2.5}$ on the polluted day was significantly higher than that on the non-polluted day, with a difference of about 25 μg/m^3. On pollution days, $PM_{2.5}$ concentrations peaked at 57 μg/m^3 at 9:00 a.m. On clean days, $PM_{2.5}$ concentrations peaked at 31 μg/m^3 at 8:00 a.m. The peak $PM_{2.5}$ concentration on polluted days lagged one hour behind that on clean days, and the increase was significantly.

On polluted days, the proportions of $PM_{2.5}$ components in decreasing order were organic matter (30.81%), NO_3^- (20.47%), SO_4^{2-} (15.09%), NH_4^+ (13.98%), others (9.95%), EC (3.97%), Ca^{2+} (2.55%), Cl^- (1.22%), K^+ (1.16%), Na^+ (0.50%), and Mg^{2+} (0.30%) (Figure 6). On clean days, the proportions of $PM_{2.5}$ components in decreasing order were organic matters (29.55%), SO_4^{2-} (15.82%), NO_3^- (15.67%), NH_4^+ (12.74%), others (10.49%), EC (6.16%), Ca^{2+} (4.61%), Cl^- (1.86%), K^+ (1.36%), Na^+ (1.09%), and Mg^{2+} (0.65%) (Figure 6). The level of NO_3^- on polluted days were higher than those on clean days, with a difference of about 5%. The proportions of organic matters and NH_4^+ were about 1% higher on polluted days than those on clean days. The level of EC and Ca^{2+} on clean days were higher than those on polluted days, with a difference of about 2%. The proportions of Cl^-, K^+, Na^+, and Mg^{2+} on clean days were higher than those on polluted days.

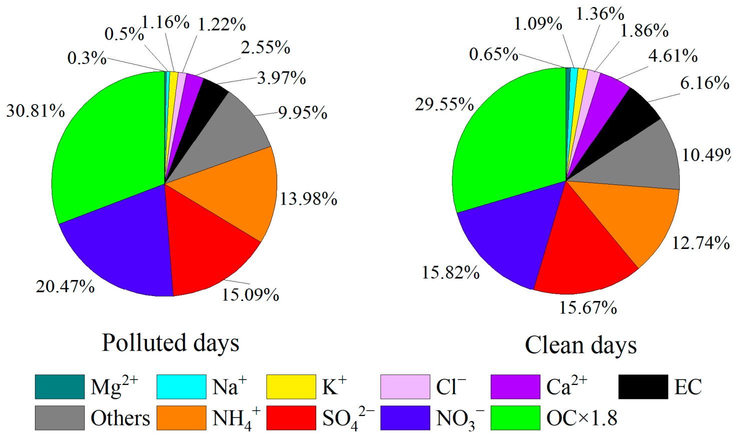

Figure 6. Proportions of $PM_{2.5}$ components on the polluted and clean days in Dongying in September 2022.

3.2.2. Spatial Variation

During episode I (Figure 7), the daily concentration of O_3 in Dongying showed a distribution characteristic of "low in the north and high in the south" from 7 to 10 September. The O_3 concentration increase began in the south of Dongying. With the development of O_3 pollution, it reached more than 232 μg/m^3 in the southern areas on 9 September, which was seriously polluted. On 10 September, the overall pollution situation improved, but it still exceeded 196 μg/m^3 in most areas. On 11 September, the levels of O_3 were 160–178 μg/m^3 in all areas except in the north-central region, which were still 196 μg/m^3. On 12 September, the O_3 concentration rebounded, showing a distribution characteristic of "low in the north and high in the south". On 13 September, it dropped to below 160 μg/m^3, and O_3 did not exceed the standard limit. Based on the distribution characteristics of $PM_{2.5}$ concentration, the variation trend of $PM_{2.5}$ concentration was consistent with that of O_3 in Dongying from 7 to 13 September. The spatial variation of $PM_{2.5}$ concentration was low on 7, 8, and 13 September, but high on 9, 10, 11, and 12 September. The concentration of $PM_{2.5}$ on 9 September was high in the north and low in the south, while it was low in the north and high in the south on 10, 11, and 12 September. The overall concentration distribution characteristics were similar to those of O_3.

During episode II (Figure 7), the O_3 concentration in Dongying was less than 160 μg/m^3 on 24 September, not exceeding the standard limit. From 25 to 28 September, O_3 pollution gradually increased. On 25 September, the daily high value of O_3 appeared in the northeast region, and then O_3 concentration gradually increased on 26 and 27 September, showing an overall distribution characteristic of "high in the south and low in the north". On 28 September, the O_3 concentration in most areas of Dongying was higher than 232 μg/m^3. From 29 to 30 September, the O_3 pollution situation was improved, but the O_3 concentration in the northern area was still higher than 232 μg/m^3, with a distribution characteristic of "high in the north and low in the south". Based on the distribution characteristics of $PM_{2.5}$ concentration, the variation trend of $PM_{2.5}$ concentration was consistent with that of O_3 concentration in Dongying from 20 to 30 September. Overall, the concentration of $PM_{2.5}$ in Dongying showed a distribution characteristic of "high in the north and low in the south", which was similar to the concentration distribution characteristics of O_3.

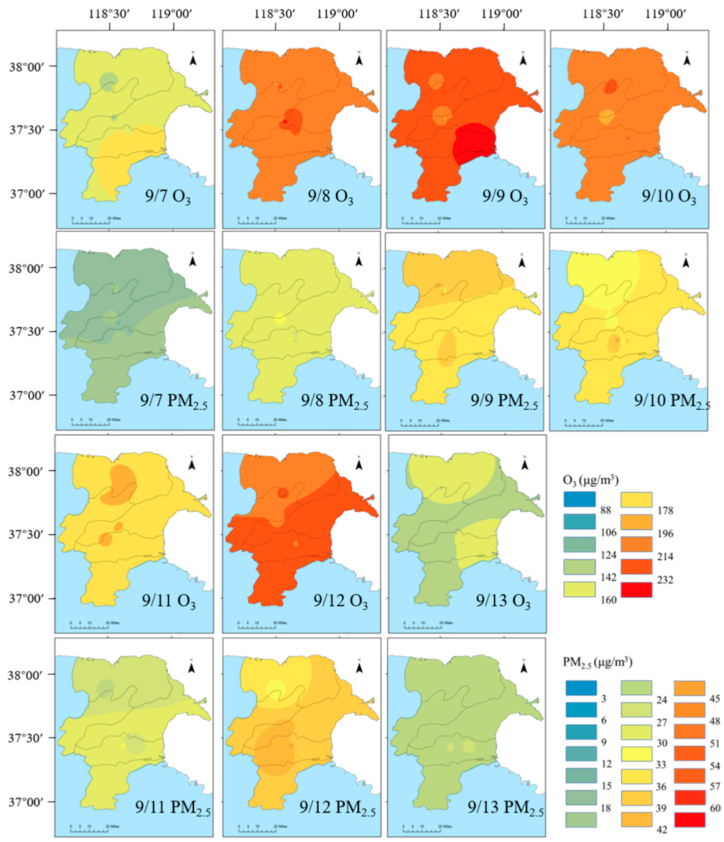

Figure 7. *Cont.*

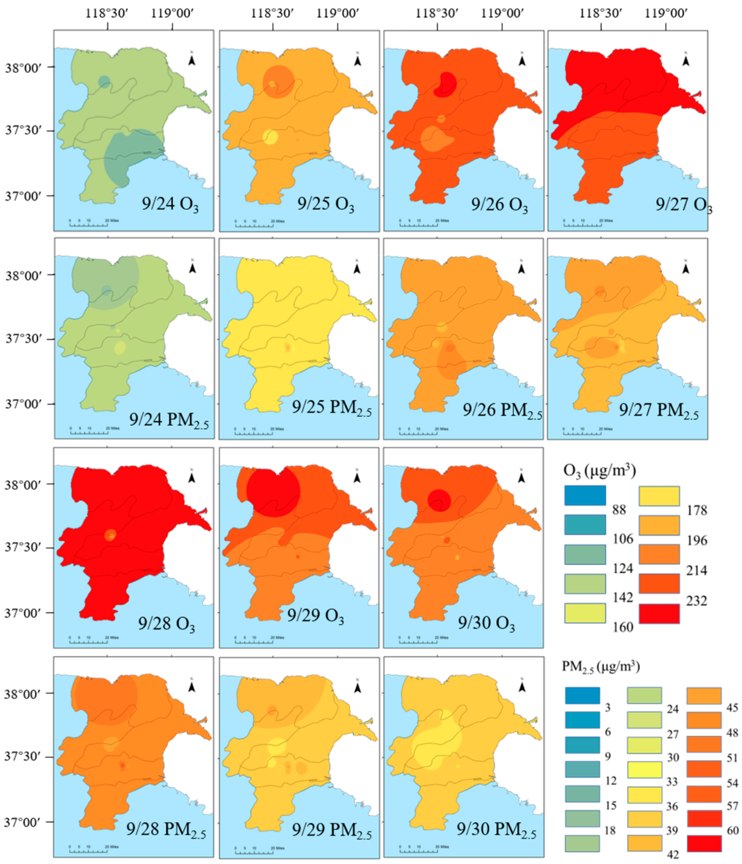

Figure 7. Spatial and temporal distribution of $PM_{2.5}$ and O_3 from 7 to 13 September 2022 and 24 to 30 September 2022.

3.2.3. Correlation Analysis of $PM_{2.5}$ and O_3

In September 2022, the Pearson correlation coefficient of O_3 and $PM_{2.5}$ was 0.92 in Dongying, showing a strong positive correlation (Figure 8). The Pearson correlation coefficient between O_3 and $PM_{2.5}$ was 0.84 and 0.64 on polluted and clean days, respectively. The positive correlation between O_3 and $PM_{2.5}$ was stronger on polluted days. In pollution days of episode I and II, the Pearson correlation coefficients of O_3 and $PM_{2.5}$ were 0.71 and 0.87, respectively. Compared with Episode I, which was dominated by light pollution, the correlation between O_3 and $PM_{2.5}$ was stronger in Episode II, which was dominated by moderate pollution, indicating that the correlation between O_3 and $PM_{2.5}$ was stronger with the increase in pollution level.

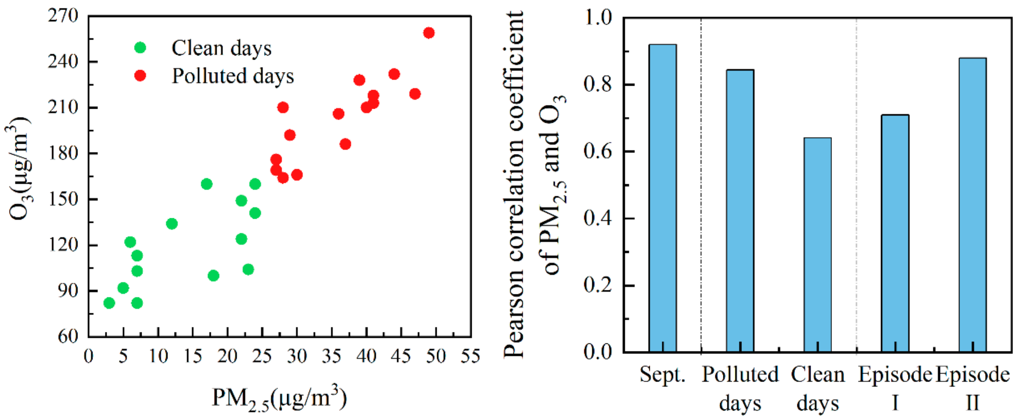

Figure 8. Correlation analysis of $PM_{2.5}$ and O_3 in Dongying in September 2022.

3.3. Cause Analysis of Complex Pollutions

3.3.1. Meteorological Conditions of Pollutions

The meteorological factors (temperature, relative humidity, wind speed, air pressure, and ultraviolet radiation) of polluted days and clean days were comparatively analyzed in Dongying in September 2022 (Figure 9). The results showed that the daily average temperature of polluted days (range: 20.0–25.8 °C, mean: 22.6 °C) was slightly higher than that of clean days (range: 17.3–25.0 °C, mean: 21.0 °C). The daily average relative humidity (range: 51.9–73.0%, mean: 62.1%) was lower than that of clean days (range: 34.2–94.0%, mean 64.5%), indicating that high temperature and low humidity were conducive to the formation of O_3 pollution. The humidity at nighttime on polluted days was higher than that on clean days, which was conducive to the generation of particulate matters.

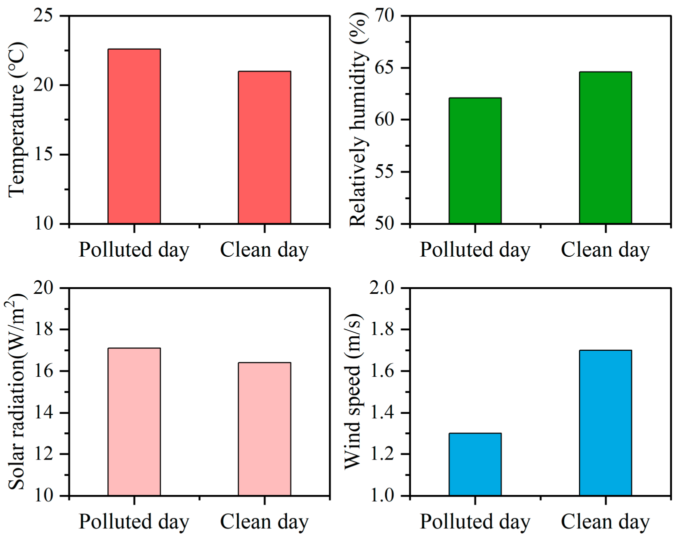

Figure 9. Comparison of meteorological conditions on polluted and clean days in September 2022.

The daily average atmospheric pressure on polluted days (range: 1007.0–1018.0 hPa, mean: 1013.0 hPa) varied a little compared with that on clean days (range: 1004.7–1017.8 hPa, mean: 1013.5 hPa). Wind speed on polluted days (range: 0.7–2.3 m/s, mean: 1.3 m/s) was lower than that on clean days (range: 0.8–32.9 m/s, mean: 1.7 m/s). The dominant wind direction on polluted days was south wind, and the dominant wind direction on clean days was northeast wind. The diffusion conditions were poor at low wind speeds, and pollutants continued to accumulate locally. The daily average radiation flux on polluted days (UV-A: 14.4–19.3 W/m^2, mean: 17.1 W/m^2) was higher than that on clean days (UV-A: 6.9–22.7 W/m^2, mean: 16.9 W/m^2), and the high radiation flux was beneficial to the formation of O_3.

In general, the main meteorological conditions for $PM_{2.5}$ and O_3 pollution in Dongying in September were higher daytime temperature, nighttime relative humidity and radiation flux, and lower speed south wind and southeast wind superimposed convergence zone.

3.3.2. Local Emissions

In September 2022, the average daily emissions of NO_x, SO_2, smoke dust, and total non-methane hydrocarbons were 22.62, 8.70, 0.99, and 0.55 tons in Dongying, respectively (Figure S5). The average daily emissions of these four types of pollutants on pollution days were lower than those on clean days. The emissions of NO_x, SO_2, and smoke dust in Episode II with moderate pollution was lower than that in Episode I with light pollution, indicating that the complex pollution process in September was more likely to be affected by meteorological conditions and transmission than by local emissions.

Model simulation results show that, in September 2022, O_3 in Dongying mainly came from industrial sources (29% ± 12%) and transportation sources (18% ± 10%) (Figure 10).

The precursor NO_x was mainly from industrial sources (49% ± 12%) and transportation sources (29% ± 13%), and VOCs were mainly from industrial sources (59% ± 13%) and transportation sources (14% ± 7%) (Figure 10). During episode I, the industrial sources were the primary contributors of O_3, NO_x, and VOCs, with relative contributions of 36%, 48%, and 64%, respectively. Transportation sources were the second contributors to O_3, NO_x, and VOCs, with relative contributions of 23%, 29%, and 17%, respectively. Compared with the average values in September, the relative contribution of industrial sources to O_3 and VOCs during Episode I increased by 5% and 7%, but decreased by 1% for NO_x; the relative contribution of transportation sources to O_3 and VOCs increased, and the relative contribution to NO_x remained flat. During episode II, industrial and transportation sources were still the major contributors to O_3, NO_x, and VOCs in Dongying. Compared with the average values of Episode I, the relative contributions of industrial sources to O_3, NO_x, and VOCs decreased by 2–4%, while the contributions of transportation sources increased by 1–5%. It can be seen that the level of O_3 and the precursors NO_x and VOCs in Dongying is mainly influenced by industrial and transportation sources.

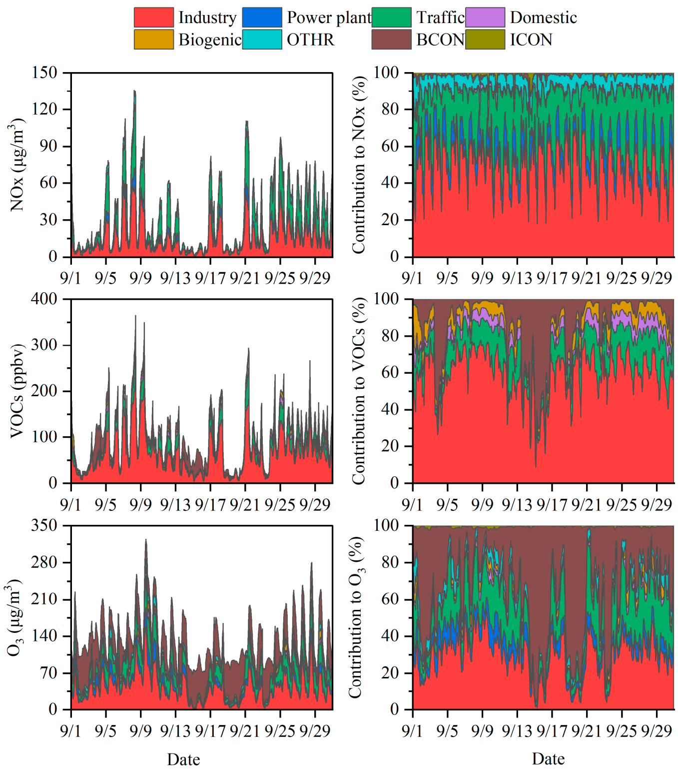

Figure 10. Absolute and relative contributions of different sources to the near-surface NO_x, VOCs, and O_3 at the Atmospheric Observatory of Dongying in September 2022. OTHR, BCON, and ICON denote contribution from other areas, boundary condition, and initial condition, respectively.

3.3.3. Chemical Transformation

O_3

In September 2022, the O_3 formation on polluted and clean days in Dongying was in the transitional and NO_x-limited regimes, respectively (Figure 11). The control of NO_x and VOCs on polluted days could effectively reduce the O_3 concentration. The sensitivity of O_3 formation to NO_x decreased and that to VOCs increased on polluted days compared with clean days. The diurnal variation of the sensitivity of O_3 formation showed that NO_x had an inhibitory effect on O_3 formation before 11:00 on the polluted days, which was in the VOCs-limited regimes, and it was in the transitional regimes after 11:00 (Figure 12). On clean days, both NO_x and VOCs promoted O_3 formation in the daytime, and O_3 formation was more sensitive to NO_x from 10:00 and in the NO_x-limited regimes from 10:00 to 17:00.

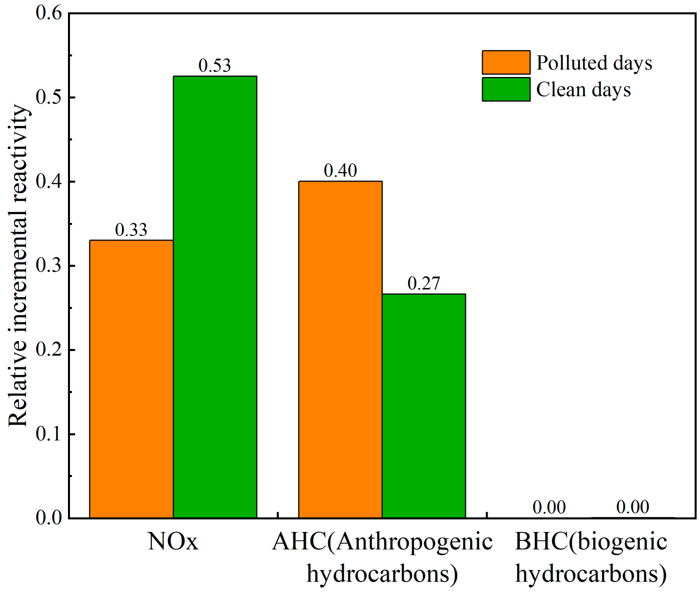

Figure 11. Sensitivity of O_3 formation in Dongying in September 2022.

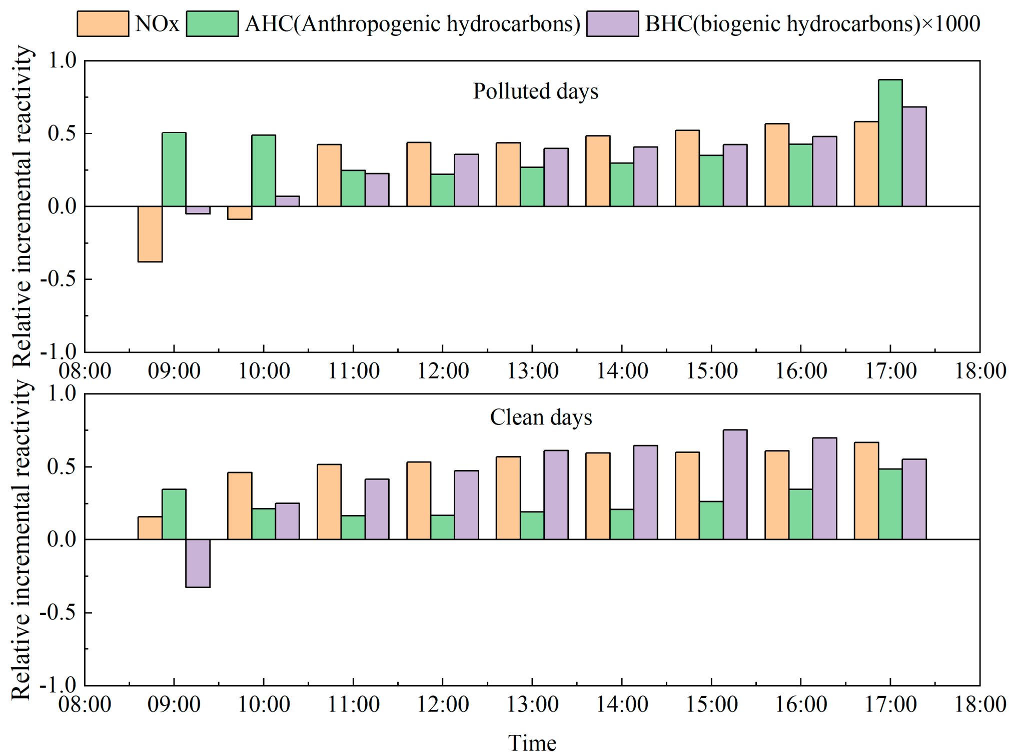

Figure 12. Diurnal variation of sensitivity of O_3 formation in Dongying in September 2022.

According to the simulated net formation rate of O_3, the average net formation rate of O_3 was 25.7 ppbv/h from 9:00 to 17:00 on polluted days, which was significantly higher than 17.0 ppbv/h on clean days (Figure 13). The maximum net formation rate of O_3 on polluted days was 50.6 ppbv/h, which was slightly higher than that on clean days (48.7 ppbv/h). The local formation promoted the increase in O_3 concentration on polluted days in Dongying.

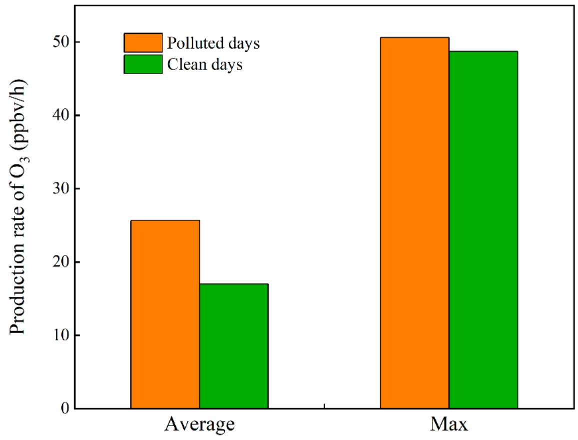

Figure 13. Comparison of diurnal net formation rate of O_3 concentration on polluted and clean days in Dongying in September 2022.

$PM_{2.5}$

In September 2022, with the development of O_3 pollution, the concentrations of NO_3^- and SO_4^{2-} in $PM_{2.5}$ increased to different degrees (Figure S6). From the hourly variations of SO_2 and NO_2 concentrations, the variation trend of SO_4^{2-} concentration was relatively consistent with that of SO_2 concentration, and the Pearson correlation coefficient was 0.21 (Figure 14). The variation trend of NO_3^- concentration was consistent with that of NO_2, and the Pearson correlation coefficient was 0.32 (Figure 14). In general, with the concentration increases of precursors NO_2 and SO_2, the concentrations of NO_3^- and SO_4^{2-} in $PM_{2.5}$ increased significantly. The concentration increases of precursors NO_2 and SO_2 contributed greatly to the formation of NO_3^- and SO_4^{2-} during the pollution period in Dongying.

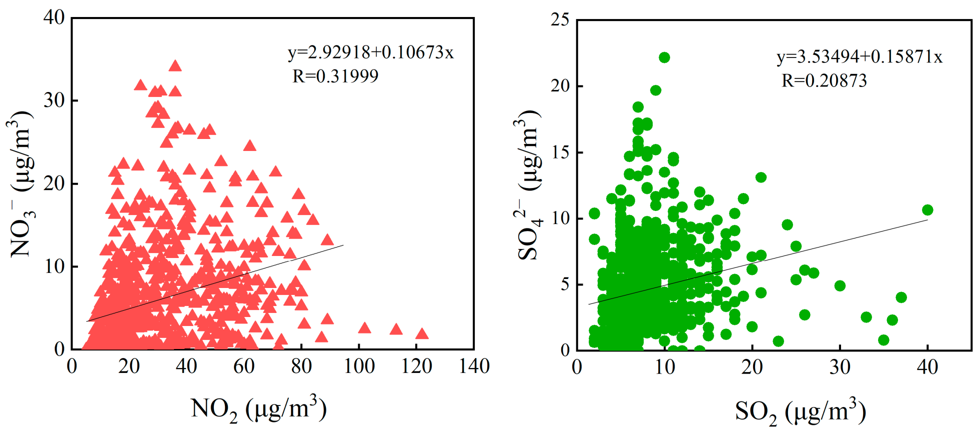

Figure 14. Scatter plot of NO_2-NO_3^- and SO_2-SO_4^{2-} in Dongying in September 2022.

In September 2022, when the hourly concentration of $PM_{2.5}$ increased, the concentrations of OC and SOC in Dongying increased significantly (Figure S7). The average SOC/OC was 71.8% ± 15.4%, with a range of 3.1% to 93.8% (Figure 15). The average proportion of SOC in $PM_{2.5}$ was 13.1% ± 5.2%, with a range of 0.3% to 52.2% (Figure 15). Compared with clean days, the average proportion of SOC in OC and $PM_{2.5}$ increased by 14% and 2.3%, respectively, on polluted days. During the two episodes, the proportion of SOC in OC and $PM_{2.5}$ also increased; in particular, in episode II, which included four moderate pollution days, the proportion of SOC in $PM_{2.5}$ increased by 5.5% compared with the clean day, indicating that SOC contributed significantly to $PM_{2.5}$ on polluted days, especially on moderately polluted days.

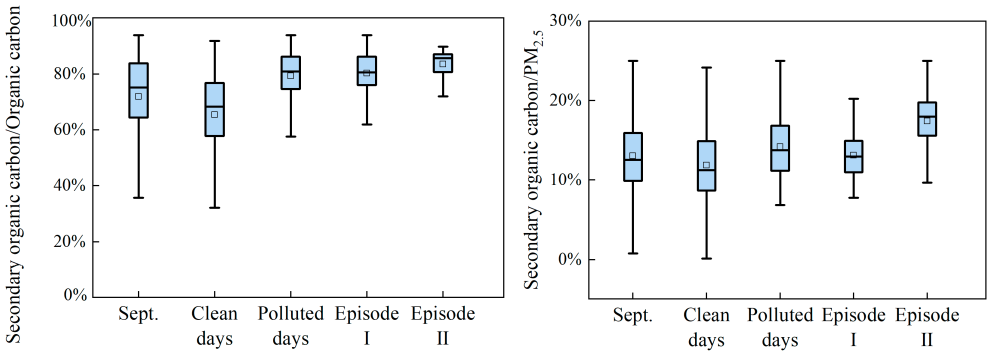

Figure 15. Proportion of SOC in OC and $PM_{2.5}$ in September 2022.

Effect of Atmospheric Oxidation on the Formation of Secondary Inorganic Components in $PM_{2.5}$

The peak hourly concentration of O_X increased from 181 μg/m^3 to 278 μg/m^3 from 1 to 8 September and remained at a high level (210–260 μg/m^3) from 9 to 12 September (Figure 16). On 13 September, it decreased to 136 μg/m^3. It fluctuated between 85 μg/m^3 and 186 μg/m^3 from 14 to 24 September, and the peak value was relatively low. The peak hourly O_X concentration increased again from 25 to 28 September (193–277 μg/m^3) and decreased slightly to 221–223 μg/m^3 from 29 to 30 September. Overall, the hourly concentration of O_X varied greatly during the O_3 pollution process.

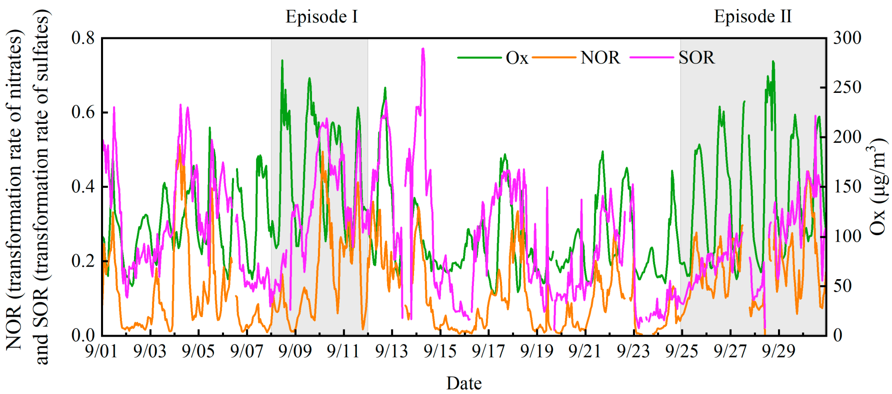

Figure 16. Time series diagram of NOR, SOR and O_X in Dongying in September 2022.

The variation trends of SOR and NOR were consistent with that of O_X (Pearson correlation coefficients were 0.36 and 0.28, respectively) (Figure 16). In general, the variation relationship among O_X, SOR and NOR reflected that the process of accelerated transformation of primary pollutants such as SO_2 and NO_2 was caused by strong atmospheric photochemical reactions. This process led to the conversion of precursors such as NO_2 and SO_2 to NO_3^- and SO_4^{2-} in the O_3 pollution process, which increased the concentration of secondary inorganic components in $PM_{2.5}$. In the early stage of Episode I, O_x was at a high level, indicating that the overall atmospheric oxidation was enhanced, and SOR and NOR increased accordingly. During Episode II, the O_X, SOR, and NOR all maintained high levels, indicating that the increase in O_X atmospheric oxidation was an important reason for the increase in NO_3^- and SO_4^{2-} concentrations in $PM_{2.5}$.

3.3.4. Air pollution Transportations

In September 2022, O_3 pollutions occurred frequently in central and eastern China. Under the influence of southerly wind, Dongying continued to be in the downwind direction of the polluted area.

The results of backward trajectory cluster analysis showed that it was affected by air mass transportations in multiple directions during the two episodes in Dongying, mainly in the southwest and southeast directions (Figures S8 and S9). Moreover, in one episode, the source direction of the polluted air masses continuously varied, which made the formation of a convergence zone easy and the diffusion of pollutants difficult. In addition, the transportation path of the polluted air masses passed through the Bohai Bay, which makes Dongying vulnerable to the influence of maritime pollution transportation. The vertical observations showed that $PM_{2.5}$ and O_3 accumulated near the surface and were transported vertically during both pollution periods (Figure S10). This indicated that the complex air pollution in Dongying was not only affected by horizontal transportation, but also by vertical transportation.

Model simulations show that in September 2022, O_3 in Dongying was mainly from local contribution (19% ± 13%) and Jinan, Tai'an, Zibo, and Weifang (19% ± 20%) in Shandong. Precursor NO_x was mainly from Jinan, Tai'an, Zibo, and Weifang in Shandong (20% ± 24%) in addition to local contribution (69% ± 24%). VOCs were also mainly from Jinan, Tai'an, Zibo, and Weifang in Shandong (24% ± 25%) in addition to local contribution (42% ± 21%) (Figure 17). It has been shown that Zibo, Jinan, and Weifang in Shandong Province have high emission intensity of VOCs, and Weifang also has high VOCs emissions. The main sources of VOCs in these cities were solvent usage, industrial processes, and road-mobile sources. The NOx emission intensities of Jinan and Zibo ranked among the top three in Shandong Province (25.9 and 19.1 t/km^2, respectively), which were higher than the average value of Shandong Province (18.4 t/km^2). NO_x in these cities mainly comes from fossil fuel combustion and road-mobile sources [35]. When the dominant wind direction in the region was southwest–southeast, the above areas being located upwind of Dongying meant that Dongying was susceptible to impacts on air quality.

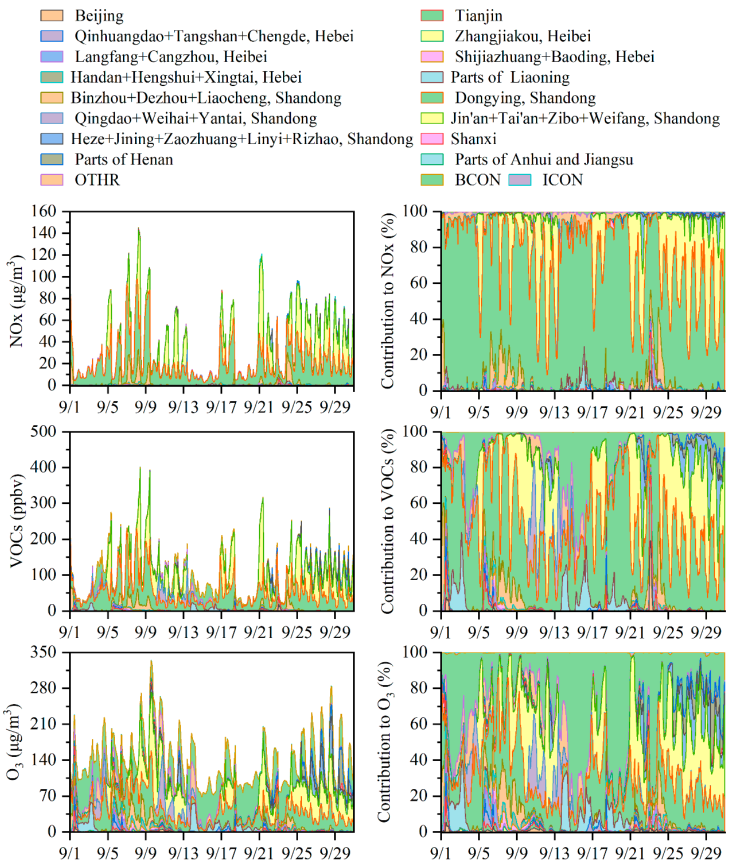

Figure 17. Absolute and relative contributions of each marked regions to the near-surface NO_x, VOCs, and O_3 at the Atmospheric Observatory of Dongying in September 2022. OTHR, BCON, and ICON denote contribution from other areas, boundary condition, and initial condition, respectively.

During Episode I, Jinan, Tai'an, Zibo, and Weifang in Shandong had the highest relative contribution to O_3 in Dongying (32%), with an increase of more than 13% compared to clean days, followed by Dongying's local generation (20%), with no significant change compared to clean days. NO_x was mainly affected by local emissions (64%), but the relative contribution decreased by more than 5% compared to clean days, followed by Jinan, Tai'an, Zibo, and Weifang in Shandong (26%), with an increase of more than 6% compared with clean days. VOCs were mainly affected by local emissions and Jinan, Tai'an, Zibo, and Weifang in Shandong, which contributed 35% and 36% to VOCs in Dongying, respectively. Compared with clean days, the local contribution decreased by more than 7%, and the influence of Shandong Jinan, Tai'an, Zibo, and Weifang increased by more than 12%.

Compared with Episode I, the contribution of local generation to O_3 in Dongying during Episode II was flat, the contribution of Jinan, Tai'an, Zibo, and Weifang in Shandong increased by 3%, and the contribution of Heze, Jining, Zaozhuang, Linyi, and Rizhao in Shandong Province increased from 3% to 12%; the contribution of local generation to NO_x in Dongying decreased to 52%, and the contribution of Jinan, Tai'an, Zibo, and Weifang in Shandong Province increased to 40%; the contribution of local generation to VOCs in Dongying decreased by 2%, while that of Jinan, Tai'an, Zibo, and Weifang in Shandong, and that of Heze, Jining, Zaozhuang, Linyi, and Rizhao in Shandong increased by 8% and 11%, respectively. It can be seen that the contribution of regional transportation to O_3 and precursors NO_x and VOCs increased significantly during the pollution period, and regional joint prevention and control is very important for air pollution prevention and control in Dongying.

4. Conclusions

Under the background of a widespread regional air pollution process in the central and eastern regions of China, two complex air pollution episodes with a duration of 5–6 days occurred in Dongying in September 2022. The hourly concentrations of O_3 and $PM_{2.5}$ were in the ranges of 8–275 and 2–86 $\mu g/m^3$, respectively. The causes of pollution are as follows.

- Higher daytime temperatures, higher nighttime relative humidity, high radiative fluxes, and low-speed southerly and southeasterly winds superimposed on the convergence zone are the main pollution meteorological conditions for the $PM_{2.5}$ and O_3 complex pollution in Dongying in September.
- In the context of pollutant emissions at a high level, compared with the variations in precursors emissions, the complex air pollution episode in September is more susceptible to changes in meteorological conditions and pollutant transport.
- The net daytime O_3 generation rate in Dongying on polluted days was twice as high as that on clean days; O_3 generation in the daytime was in the transitional regimes, and in the VOCs-limited regimes in the morning. The concentration increases of precursors NO_2 and SO_2 contributed greatly to the formation of NO_3^- and SO_4^{2-}. When O_3 was formed via atmospheric photochemical reactions, the atmospheric oxidation capacity was also improved, which promoted the conversion of precursors such as NO_2 and SO_2 to NO_3^- and SO_4^{2-}. On the polluted days, secondary organic matter contributed significantly to the increase in $PM_{2.5}$ concentration, which together led to the increasing trend of secondary pollutants concentrations in the process of O_3 pollution.
- In addition, Dongying was frequently in the downwind direction of land and sea and was often in the convergence zone of air flows during the episodes. The diffusion conditions were very poor, and thus the pollutants formed locally and transported from the upwind direction, including the Bohai Bay air mass transportation, were easy to be accumulated. The vertical transportation would further increase the concentration of pollutants in Dongying.

Synergistic control of complex air pollution is the focus of air pollution management in China in the future. In order to improve ambient air quality and protect human health, here are some policy recommendations for Dongying.

- In terms of control, (1) the synergistic control of NO_x and VOCs at the city level should be further strengthened in Dongying, and in particular, the control of NO_x and VOCs emissions at nighttime needs to be strengthened to minimize the impact on O_3 and $PM_{2.5}$ complex pollution. (2) It is recommended that Dongying local government should actively promote the construction of effective air pollution joint prevention and control mechanisms with the neighboring cities such as Jinan, Tai'an, Zibo, and Weifang in Shandong Province.
- In terms of research, attention should be paid to scientific research on the characteristics of atmospheric pollution in Bohai Bay and its impact on the air quality of coastal cities, so as to contribute to the effective improvement of ambient air quality in coastal cities in Bohai Bay Rim.

Supplementary Materials: The following supporting information can be downloaded at: https://www.mdpi.com/article/10.3390/atmos15010073/s1, Figure S1: Daily variations of $PM_{2.5}$ and MDA8-O_3 in Dongying in 2022; Figure S2: Simulated regions for source apportionment of O_3; Figure S3: Daily variation of ambient air quality in Dongying City in September 2022; Figure S4: Diurnal variation of ultraviolet radiation in Dongying City in September 2022; Figure S5: Comparison of pollution source emissions in Dongying in September 2022; Figure S6: Time series of SO_2, NO_2, NO_3^- and SO_4^{2-} in Dongying in September 2022; Figure S7: Time series diagram of SOC, OC and $PM_{2.5}$ concentrations in Dongying in September 2022; Figure S8: Results of backward trajectory cluster analysis during Sep. 8th to 12th; Figure S9: Results of backward trajectory cluster analysis during Sep. 25th to 30th; Figure S10: Vertical distribution characteristics of O_3 and $PM_{2.5}$ in Dongying in September 2022; Table S1: Air quality sub-index (IAQI)and the corresponding pollutant concentration limits.

Author Contributions: Conceptualization, H.L.; Formal analysis, J.T., J.L. (Jialin Li), X.Y. and W.C.; Funding acquisition, F.S. and J.L. (Jidong Li); Methodology, R.G. and F.B.; Software, X.G., X.Z. and L.T.; Supervision, H.L.; Writing—original draft, Y.J. and C.A.; Writing—review and editing, Y.J. All authors have read and agreed to the published version of the manuscript.

Funding: This work is supported by the Ministry of Ecology and Environment of China under the project (DQGG202121), the Fundamental Research Funds for the Central Public-interest Scientific Institution (2023YSKY-14), and Dongying Ecological and Environmental Bureau (2021DFKY-0779).

Institutional Review Board Statement: Not applicable.

Informed Consent Statement: Not applicable.

Data Availability Statement: The data presented in this study are available in "Causes investigation of $PM_{2.5}$ and O_3 complex pollution in a typical coastal city in the Bohai Bay region of China in autumn: Based on one-month continuous intensive observation and model simulation".

Conflicts of Interest: Author Luyao Tan was employed by the company Ltd. of Shandong Environmental Protection Industry Corp. The remaining authors declare that the research was conducted in the absence of any commercial or financial relationships that could be construed as a potential conflict of interest.

References

1. He, J.; Gong, S.; Yu, Y.; Yu, L.; Wu, L.; Mao, H.; Song, C.; Zhao, S.; Liu, H.; Li, X.; et al. Air pollution characteristics and their relation to meteorological conditions during 2014-2015 in major Chinese cities. *Environ. Pollut.* **2017**, *223*, 484–496. [CrossRef]
2. Li, R.; Wang, Z.; Cui, L.; Fu, H.; Zhang, L.; Kong, L.; Chen, W.; Chen, J. Air pollution characteristics in China during 2015-2016: Spatiotemporal variations and key meteorological factors. *Sci. Total Environ.* **2019**, *648*, 902–915. [CrossRef] [PubMed]
3. Tang, X.Y.; Zhang, Y.H.; Shao, M. *Atmospheric Environmental Chemistry*, 2nd ed.; High Education Press: Beijing, China, 2006.
4. Dai, S. *Advances in Environmental Chemistry*; Chemical Industry Press: Beijing, China, 2005.
5. Zeng, Y.; Cao, Y.; Qiao, X.; Seyler, B.C.; Tang, Y. Air pollution reduction in China: Recent success but great challenge for the future. *Sci. Total Environ.* **2019**, *663*, 329–337. [CrossRef] [PubMed]
6. Lyu, X.P.; Chen, N.; Guo, H.; Zhang, W.H.; Wang, N.; Wang, Y.; Liu, M. Ambient volatile organic compounds and their effect on ozone production in Wuhan, central China. *Sci. Total Environ.* **2016**, *541*, 200–209. [CrossRef] [PubMed]
7. Lyu, X.; Wang, N.; Guo, H.; Xue, L.; Jiang, F.; Zeren, Y.; Cheng, H.; Cai, Z.; Han, L.; Zhou, Y. Causes of a continuous summertime O3 pollution event in Jinan, a central city in the North China Plain. *Atmos. Chem. Phys.* **2019**, *19*, 3025–3042. [CrossRef]

8. Zhao, H.; Chen, K.; Liu, Z.; Zhang, Y.; Shao, T.; Zhang, H. Coordinated control of $PM_{2.5}$ and O_3 is urgently needed in China after implementation of the "Air pollution prevention and control action plan". *Chemosphere* **2021**, *270*, 129441. [CrossRef] [PubMed]
9. Yang, C.; Yang, H.; Guo, S.; Wang, Z.; Xu, X.; Duan, X.; Kan, H. Alternative ozone metrics and daily mortality in Suzhou: The China Air Pollution and Health Effects Study (CAPES). *Sci. Total Environ.* **2012**, *426*, 83–89. [CrossRef]
10. Yue, X.; Unger, N. Ozone vegetation damage effects on gross primary productivity in the United States. *Atmos. Chem. Phys.* **2014**, *14*, 9137–9153. [CrossRef]
11. Dong, C.; Gao, R.; Zhang, X.; Li, H.; Wang, W.; Xue, L. Assessment of O_3-induced crop yield losses in northern China during 2013–2018 using high-resolution air quality reanalysis data. *Atmos. Environ.* **2021**, *259*, 118527. [CrossRef]
12. Feng, Z.; De Marco, A.; Anav, A.; Gualtieri, M.; Sicard, P.; Tian, H.; Fornasier, F.; Tao, F.; Guo, A.; Paoletti, E. Economic losses due to ozone impacts on human health, forest productivity and crop yield across China. *Environ. Int.* **2019**, *131*, 104966. [CrossRef]
13. Liu, C.; Chen, R.; Sera, F.; Vicedo-Cabrera, A.M.; Guo, Y.; Tong, S.; Lavigne, E.; Correa, P.M.; Ortega, N.V.; Achilleos, S.; et al. Interactive effects of ambient fine particulate matter and ozone on daily mortality in 372 cities: Two stage time series analysis. *BMJ* **2023**, *383*, e075203. [CrossRef] [PubMed]
14. Jiang, H.; Gao, J.; Li, H.; Chu, W.; Chai, F. Preliminary Research on Theoretical Framework of Cooperative Control of AirPollution in China. *Res. Environ. Sci.* **2022**, *35*, 601–610. [CrossRef]
15. Li, H.; Peng, L.; Bi, F.; Li, L.; Bao, J.; Li, J.; Zhang, H.; Chai, F. Strategy of Coordinated Control of PM2. 5 and Ozone in China. *Res. Environ. Sci.* **2019**, *32*, 1763–1778. [CrossRef]
16. Hua, C.; Jiang, Q.; Chi, X.; Liu, C. Meteorological Characteristics of $PM_{2.5}$-O_3 Air Combined Pollution in Central andEastern China in the Summer Half Years of 2015–2020. *Res. Environ. Sci.* **2022**, *35*, 650–658. [CrossRef]
17. Jia, M.; Zhao, T.; Cheng, X.; Gong, S.; Zhang, X.; Tang, L.; Liu, D.; Wu, X.; Wang, L.; Chen, Y. Inverse Relations of $PM_{2.5}$ and O_3 in Air Compound Pollution between Cold and Hot Seasons over an Urban Area of East China. *Atmosphere* **2017**, *8*, 59. [CrossRef]
18. Zhu, J.; Chen, L.; Liao, H.; Dang, R. Correlations between PM2.5 and Ozone over China and Associated Underlying Reasons. *Atmosphere* **2019**, *10*, 352. [CrossRef]
19. Meng, Z.; Dabdub, D.; Seinfeld, J.H. Chemical coupling between atmospheric ozone and particulate matter. *Science* **1997**, *277*, 116–119. [CrossRef]
20. Xing, J.; Wang, J.; Mathur, R.; Wang, S.; Sarwar, G.; Pleim, J.; Hogrefe, C.; Zhang, Y.; Jiang, J.; Wong, D.C.; et al. Impacts of aerosol direct effects on tropospheric ozone through changes in atmospheric dynamics and photolysis rates. *Atmos. Chem. Phys.* **2017**, *17*, 9869–9883. [CrossRef]
21. Tao, Z.; Yu, H.; Chin, M. The Role of Aerosol-Cloud-Radiation Interactions in Regional Air Quality—A NU-WRF Study over the United States. *Atmosphere* **2015**, *6*, 1045–1068. [CrossRef]
22. Li, J.; Carlson, B.E.; Yung, Y.L.; Lv, D.; Hansen, J.; Penner, J.E.; Liao, H.; Ramaswamy, V.; Kahn, R.A.; Zhang, P.; et al. Scattering and absorbing aerosols in the climate system. *Nat. Rev. Earth Environ.* **2022**, *3*, 363–379. [CrossRef]
23. Ivatt, P.D.; Evans, M.J.; Lewis, A.C. Suppression of surface ozone by an aerosol-inhibited photochemical ozone regime. *Nat. Geosci.* **2022**, *15*, 536–540. [CrossRef]
24. Zhao, M.; Shen, H.; CHen, T.; Li, J.; Sun, Z.; Ji, Y.; Xue, L.; Li, H.; Wang, W.; Shang, F. Characteristics and Sensitivity Analysis of Ozone in the Representative City of the Yellow River Delta in Summer. *Res. Environ. Sci.* **2022**, *35*, 1351–1361. [CrossRef]
25. Wu, L. Volatile Organic Compound Emissions from the Oilfield in the Yellow River Delta Region, Northern China and Their Impact on Regional Ozone Pollution. Master's Thesis, Shandong University, Jinan, China, 2019.
26. Wang, Z.S.; Chien, C.-J.; Tonnesen, G.S. Development of a tagged species source apportionment algorithm to characterize three-dimensional transport and transformation of precursors and secondary pollutants. *J. Geophys. Res.-Atmos.* **2009**, *114*, D21206. [CrossRef]
27. Kwok, R.H.F.; Napelenok, S.L.; Baker, K.R. Implementation and evaluation of $PM_{2.5}$ source contribution analysis in a photochemical model. *Atmos. Environ.* **2013**, *80*, 398–407. [CrossRef]
28. Li, Q.; Su, G.; Li, C.; Liu, P.; Zhao, X.; Zhang, C.; Sun, X.; Mu, Y.; Wu, M.; Wang, Q. An investigation into the role of VOCs in SOA and ozone production in Beijing, China. *Sci. Total Environ.* **2020**, *720*, 137536. [CrossRef] [PubMed]
29. Yin, S.; Liu, Y.; Ma, W.; Zheng, C.; Zhang, Y.; Wang, Z.; Cheng, Q.; Liu, X. Formation mechanism, precursor sensitivity and control strategies of summertime ozone on the Fenwei Plain, China. *Atmos. Environ.* **2023**, *309*, 119908. [CrossRef]
30. Xue, L.; Wang, T.; Gao, J.; Ding, A.; Zhou, X.; Blake, D.; Wang, X.; Saunders, S.; Fan, S.; Zuo, H. Ground-level ozone in four Chinese cities: Precursors, regional transport and heterogeneous processes. *Atmos. Chem. Phys.* **2014**, *14*, 13175–13188. [CrossRef]
31. Tan, Z.; Lu, K.; Jiang, M.; Su, R.; Dong, H.; Zeng, L.; Xie, S.; Tan, Q.; Zhang, Y. Exploring ozone pollution in Chengdu, southwestern China: A case study from radical chemistry to O_3-VOC-NOx sensitivity. *Sci. Total Environ.* **2018**, *636*, 775–786. [CrossRef]
32. Chow, J.C.; Watson, J.G.; Lu, Z.; Lowenthal, D.H.; Frazier, C.A.; Solomon, P.A.; Thuillier, R.H.; Magliano, K. Descriptive analysis of $PM_{2.5}$ and PM_{10} at regionally representative locations during SJVAQS/AUSPEX. *Atmos. Environ.* **1996**, *30*, 2079–2112. [CrossRef]
33. Wang, Y.Q. MeteoInfo: GIS software for meteorological data visualization and analysis. *Meteorol. Appl.* **2014**, *21*, 360–368. [CrossRef]

34. Wang, Y. An Open Source Software Suite for Multi-Dimensional Meteorological Data Computation and Visualisation. *J. Open Res. Softw.* **2019**, *7*, 21. [CrossRef]
35. Zhou, M. Emission Inventories and Pollution Characteristics of Anthropogenic Air Pollutants in Shandong Province. Master's Thesis, Jinan University, Jinan, China, 2021.